Available online at www.sciencedirect.com
ScienceDirect
Polymer 48 (2007) 3624–3631
polymer
www.elsevier.com/locate/polymer

Synthesis and crystallization behaviors of highly fluorinated aromatic polyesters

Qingzeng Zhu [a,b], Charles C. Han [a,*]

[a] State Key Laboratory of Polymer Physics and Chemistry, Joint Laboratory of Polymer Science and Materials, Beijing National Laboratory for Molecular Sciences, Institute of Chemistry, CAS, Beijing 100080, China
[b] School of Chemistry and Chemical Engineering, Shandong University, Jinan 250100, China

Received 13 February 2007; received in revised form 18 April 2007; accepted 18 April 2007
Available online 24 April 2007

Abstract

Studies on fluorine containing condensation polymers are limited compared to that of fluorine containing addition polymers. In this report, highly fluorinated aromatic polyesters were synthesized by a polycondensation reaction of tetrafluorophthalic anhydride with ethylene glycol. Viscosity, solubility, thermal properties and crystallization behaviors of fluorinated polyesters were investigated using IR, ^{19}F NMR, DSC, GPC, polarized optical microscope and rheometer. The fluorinated polyester is insoluble in most organic solvents, such as acetone, ethyl acetate, chloroform, THF, and trichloromethane. However, it is soluble in highly polar solvents, such as dimethylsulfoxide, dimethylformamide and dimethylacetamide. The fluorinated polyester (*o*-PETF) is a crystalline polymer with a crystallization enthalpy of 35.2 J/g and a broad crystallization temperature range from 54 to 130 °C. Average crystalline growth rate is 4.2 μm/min at 110 °C in the preliminary 30 min. Spherulite growth was observed at the temperature when the dendrites begin to melt. Crystallization property of *o*-PETF may be ascribed to the higher mobility of fluorinated polyester chains and dipolar contribution of carbon–fluorine bonds.

Keywords: Fluorinated polyesters; Tetrafluorophthalic anhydride; Crystallization

1. Introduction

It is a widely recognized method to modify the surface and bulk properties of polymers by introducing fluorine into polymeric chains. The fluorine atoms can confer to polymers desirable properties, such as low surface energy, thermal stability, excellent dielectric properties, good chemical resistance, low water absorption, and weatherability. These characteristics of fluorine containing polymers are imparted by the highest electron negativity (4.0), the third smallest van der Waals radius (0.135 nm), low polarizability ($\alpha = 1.27 \times 10^{-24}$ cm^3) of the fluorine atom, together with the strong bonding energy (472 kJ/mol) and the weak intermolecular cohesive energy. There has been growing interest in the synthesis of polymers containing fluorine atoms in their structure.

Introducing fluorine into polymer chains can be accomplished by several methods: such as fluorinated homopolymerization, grafting and copolymerization [1,2]. Research on fluorine containing condensation polymers is limited compared to that of fluorine containing addition polymers. This fact is due to the difficulty of extending usual methods of block copolymer synthesis because of the effect of the higher electron negativity of fluorine atoms on the fluorinated monomers in polymerization, and the difficulty in preparing fluorinated functional monomers.

Polyesters are prepared based on condensation polymerization of diols, hydroxyl-terminated polyethers or hydroquinone with diacids (derivatives). Fluorinated polyesters are expected as a source of polymers with solvent resistance, special surface properties, or prepolymers to modify other polymers. But, the synthesis of fluorinated polyesters with satisfying properties is difficult. This may arise from low reactivity of fluorinated monomers or resultant polymers' instability. Most of the

* Corresponding author. Tel.: +86 10 82618089; fax: +86 10 62521519.
E-mail address: c.c.han@iccas.ac.cn (C.C. Han).

0032-3861/$ - see front matter © 2007 Elsevier Ltd. All rights reserved.
doi:10.1016/j.polymer.2007.04.035

fluorinated polyesters studied were synthesized by condensation polymerization of hydroxyl-terminated fluorinated diols or fluorinated polyethers with non-fluorinated diacids (derivatives) [3–16]. Until recently, comparatively little research has been devoted to the condensation polymerization of fluorinated acid (derivatives) with diols or hydroxyl-terminated polyethers. Choi reported a polymerization of 4,4′-(hexafluoroisopropylidene)bis(benzoic acid) with bisphenol A [17]. Polyesters prepared from perfluoroglutartic anhydride with α,α,ω,ω-tetrahydroperfluoroglycols were mentioned [18], but no details were reported. The limited study on this route may be attributed to the scarce fluorinated diacids (derivatives) that can be offered. Tetrafluorophthalic anhydride (TFPA) now can be obtained as a commercial product. A synthesis route by which fluorine containing polyester prepared from fluorinated anhydride is explored in this paper. The properties of resultant fluorinated polyesters (*o*-PETF) from the condensation polymerization of TFPA and ethylene glycol (EG) are reported.

2. Experimental

2.1. Materials

Tetrafluorophthalic anhydride was obtained from Zhejiang Qiming Pharmaceutical Co. Ltd, China. Ethylene glycol, phthalic anhydride (PA) and organic solvents are all of reagent grade.

2.2. Fluorinated aromatic polyester synthesis

Highly fluorinated aromatic polyesters were prepared by melt polycondensation of TFPA with EG. A typical synthesis procedure is described as follows: a direct polycondensation reaction was carried out in a 150-ml round-bottomed glass reactor with a stirring assembly, a thermometer, a nitrogen gas inlet tube and a distillation condenser. High purity nitrogen was used to bubble through the reaction medium. A mixture of 44.0 g TFPA and 18.6 g EG was gradually heated from room temperature to 140 °C over a 2 h period, and then from 140 to 180 °C for 1.5 h. The reaction mixture was held at 180 °C for 3 h, then heated to 200 °C slowly and kept at 200 °C for 2 h in atmospheric pressure. At the end of the reaction, the water released by the reaction is dried off by vacuum distillation to allow the reaction to go to completion. The resultant polymers were purified to remove small molecular weight components. They were dissolved in dimethylacetamide and precipitated in excess methanol. The precipitate was washed three times with methanol and dried in a vacuum at 40 °C. A white solid was obtained. The chemical structure of *o*-PETF is presented in Scheme 1.

Non-fluorinated aromatic polyesters (*o*-PET) or non-fluorinated and fluorinated aromatic segmented co-polyesters (*o*-PETSF) were synthesized from PA, or mixtures of PA and TFPA with EG under the same conditions. Chemical structures of the *o*-PET and *o*-PETSF are presented in Schemes 2 and 3, respectively.

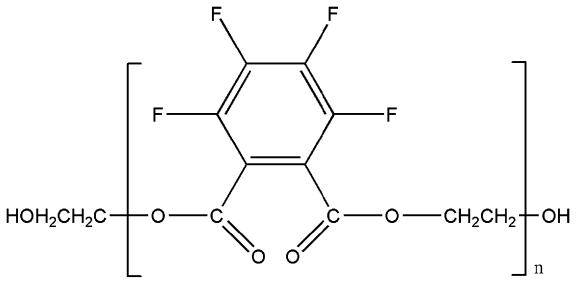

Scheme 1. Chemical structure of *o*-PETF.

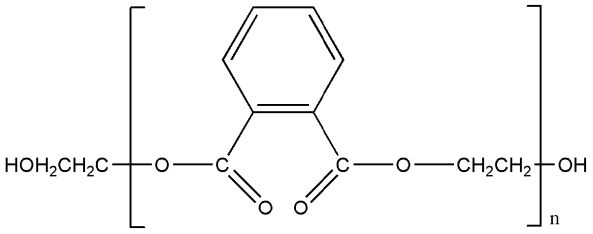

Scheme 2. Chemical structure of *o*-PET.

2.3. Measurements

IR spectra were recorded with a Bruker EQUINOX 55 FTIR spectrometer (KBr substrate). The absorption frequencies are reported in wave numbers (cm^{-1}). ^{19}F NMR spectra were obtained on a 400 MHz UltraShield™ magnet (Bruker) spectrometer, using deuterated dimethylsulfoxide (DMSO-d_6) as solvent. Thermal transitions were characterized with DSC using a Metller Toledo DSC 822^e under nitrogen in a cyclic cooling/heating program. All the specimens tested were first heated to melt and kept for 10 min to eliminate the previous thermal history. Gel permeation chromatography was performed to estimate the molecular weights of polyesters using a 1515 system GPC (Waters) equipped with 2414 refractive index and Styragel gel columns calibrated with narrow-molecular-weight polystyrene standards. Melt viscosity was measured using an ARES (TA). The polarized optical microscopic observations were carried out using a Nikon (L-UEPI) optical microscope with a Nikon (COOLPIX4500) camera. The temperature of the specimens was controlled using a Linkam LTS350 hot stage.

3. Results and discussions

3.1. Characterization

The obtained *o*-PETF is a white solid with a melt viscosity (η) of 24.5 Pa s at 130 °C. At room temperature, the *o*-PET ($\eta = 11.2$ Pa s at 90 °C) is in transparent glass state and *o*-PETSF is opaque. Comparing with *o*-PET ($M_w = 13{,}800$; polydispersity was 1.23) prepared under the same conditions, the lower molecular weight of *o*-PETF ($M_w = 8800$, polydispersity was 1.15) is partly due to the reduced reactivity of TFPA in the polycondensation reaction because of the strong electron-withdrawing influence of fluorine atoms, and the

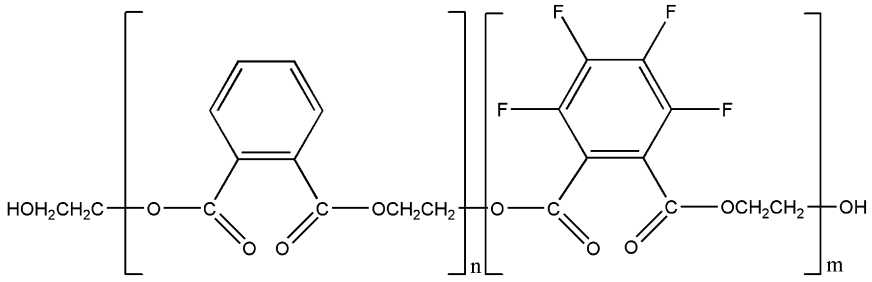

Scheme 3. Chemical structure of *o*-PETSF.

other reason may be the higher monomer molecular weight of TFPA than PA which was not included in our polystyrene equivalent molecular weight measurements obtained from GPC.

Fig. 1 shows infrared spectra of *o*-PETF and *o*-PET. IR spectrum of *o*-PETF displays absorptions associated with fluorinated aromatic nuclei. Infrared data are summarized in Table 1. The bands at 1628, 1523, 1483, 821, 788, 754 and 711 cm^{-1} arise from fluorinated aromatic nucleus vibrations. Absorption frequencies at 1325, 1223, 974 and 926 cm^{-1} are assigned to C–F stretching. ^{19}F NMR spectrum of *o*-PETF in DMSO-d_6 exhibited two signals with intensity ratio 1:1 that are attributed to the tetrafluoroaromatic ring segments in the polyester chains (Fig. 2). A septet of doublets at δ −136.4 to −139.5 ppm is assigned to the two aromatic fluorine atoms on *ortho* positions of the two carbonyls, respectively, and a long dozen of multiplets at δ −147.2 to 150.2 ppm is due to the coupling of more adjacent fluorine atoms which complicates the spectrum that is assigned to the two *meta* aromatic fluorine atoms.

3.2. Solubility

The characteristics of polymers are usually changed with substituting fluorine atoms for hydrogen atoms. One of the distinctive features of the *o*-PETF under investigation is their specific solubility. The resultant fluorinated polyester is insoluble in most organic solvents, such as acetone, ethyl acetate, chloroform, THF and trichloromethane at room temperature. However, it is soluble in highly polar solvents, such as dimethylsulfoxide, dimethylformamide and dimethylacetamide. This solubility can be ascribed to the increased polarity of polymer chains owing to the dipolar property of fluorinated segments. *o*-PET is soluble in all solvents mentioned above.

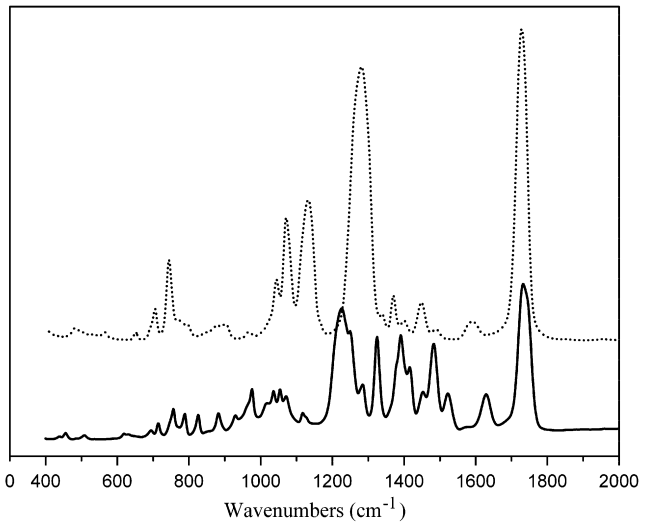

Fig. 1. Infrared spectra of *o*-PETF (bottom straight line) and *o*-PET (top dotted line).

3.3. Crystallization

3.3.1. Non-isothermal crystallization

Another distinctive feature of the *o*-PETF is crystallization. The fluorinated aromatic polyester is a high crystalline

Table 1
Assignment of bands in the infrared spectra of *o*-PETF and *o*-PET

o-PETF		*o*-PET	
Wavenumbers (cm^{-1})	Assignment	Wavenumbers (cm^{-1})	Assignment
1734	C=O	1734	C=O
1628	Fluorinated aromatic nucleus		
1523	Fluorinated aromatic nucleus	1592	Aromatic nucleus
1483	Fluorinated aromatic nucleus	1487	Aromatic nucleus
1447	CH_2	1449	CH_2
1419	CH_2	1406	CH_2
1390	CH_2	1368	CH_2
		1344	CH_2
1325	C–F stretching		
1280	Ester	1280	Ester
1223	C–F stretching		
		1130	Ester
1118	C–F, C–O		
1070	C–O–C	1070	C–O–C
1051	C–O	1044	C–O
974	C–F stretching		
926	C–F stretching		
878	CH_2	891	CH_2
821	Fluorinated aromatic nucleus		
788	Fluorinated aromatic nucleus		
754	Fluorinated aromatic nucleus	743	Aromatic nucleus
711	Fluorinated aromatic nucleus	705	Aromatic nucleus

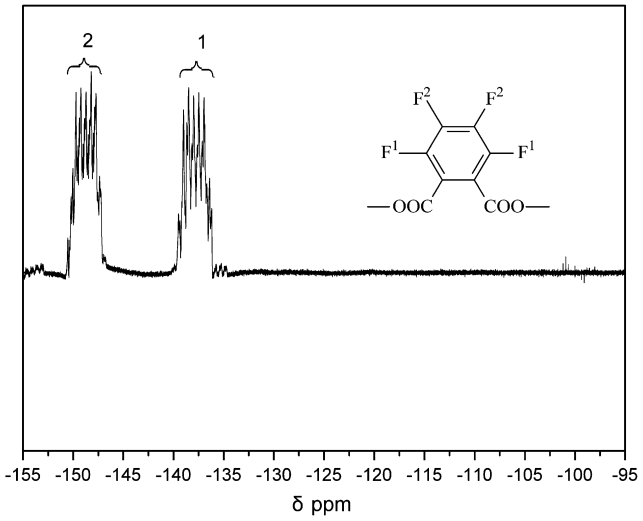

Fig. 2. ^{19}F NMR of *o*-PETF in DMSO-d_6.

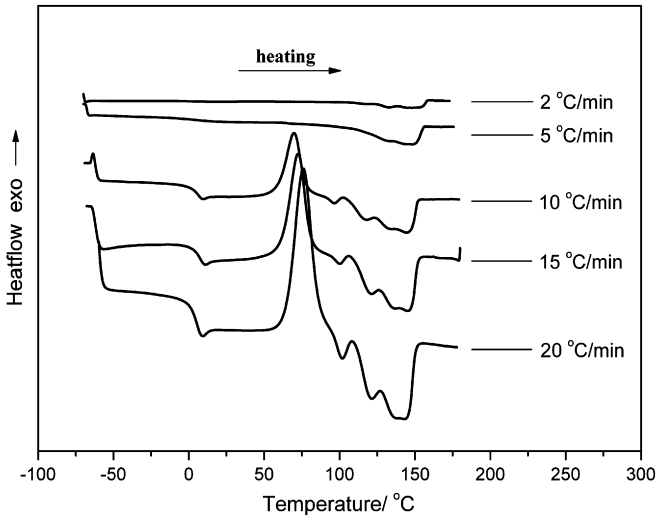

Fig. 4. DSC traces of *o*-PETF at heating rates of 2, 5, 10, 15, and 20 °C/min, N_2.

polymer. DSC was carried out from equilibrium melting state using cyclic non-isothermal programs with cooling/heating rates of 2, 5, 10, 15 and 20 °C/min. Figs. 3 and 4 show the cooling and heating DSC curves of *o*-PETF, respectively. The crystallization, glass transition, cold crystallization and melting transitions are displayed, and the corresponding thermal transition data are summarized in Table 2. The dependence of crystallization behavior on the cooling/heating rates was observed in the non-isothermal crystallization processes. At 2 and 5 °C/min cooling rates, crystallization enthalpies were 35.2 and 35.1 J/g with exothermic peaks at 103 and 94 °C, respectively. The crystallization temperature decreases with higher cooling rate partly attributed to the temperature hysteresis. During subsequent heating with the same rates, no cold crystallization peaks were observed except broad melting peaks. According to the almost constant crystallization enthalpies those were obtained at 2 and 5 °C/min cooling rates, it seems that the crystallization behavior of *o*-PETF was completed on the experimental time scale from the equilibrium liquid down to the glassy state at 2 °C/min cooling rate. So the crystallization enthalpy of the fluorinated aromatic polyester can be assigned as 35.2 J/g.

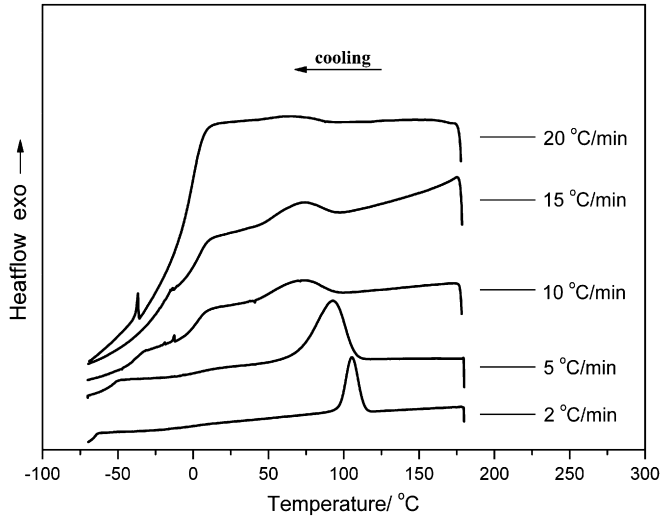

Fig. 3. DSC traces of *o*-PETF at cooling rates of 2, 5, 10, 15, and 20 °C/min, N_2.

At cooling rates of 10 and 15 °C/min, crystallization enthalpies were 6.4 and 4.2 J/g, respectively. No crystallization peaks were observed in the cooling process at a cooling rate of 20 °C/min. The gradually decreasing crystallization enthalpies with the increasing cooling rates are due to the shorter and shorter structural-relaxation time allowed for the polymer chains. The polymers could not crystallize completely without given enough time to diffuse, relax and pack into the ordered crystal structure. In the subsequent heating process with the same rates, glass transition occurred in the range of −1 to 3 °C, together with the cold crystallization in the range of 68–76 °C and broad melting peaks in the range of 105–150 °C. Dendrites were observed with polarized optical microscope at a cooling rate of 2 °C/min from the melt (Fig. 5).

Furthermore, a sample of *o*-PETF was quenched from equilibrium melting state to −70 °C at a cooling rate of 50 °C/min, and then it was heated at a rate of 2 °C/min. Figs. 6 and 7 show crystal morphology and DSC curve, respectively.

Table 2
Thermal transitions of *o*-PETF in cyclic cooling/heating programs

	2 °C/min	5 °C/min	10 °C/min	15 °C/min	20 °C/min
Cooling					
T_c (°C)	103	94	71	72	–
H_c (J/g)	35.2	35.1	6.4	4.2	–
Heating					
H_c (J/g)	–	–	23.0	32.1	29.3
T_c (°C)	–	–	68	73	76
T_m (°C)	120	120	121	122	122
	144	145	143	145	143
H_m (J/g)	38.3	41.5	33.7	34.1	27.7
T_g (°C)	–	−6	−1	2	3

T_c: crystallization temperature; H_c: crystallization enthalpy; T_m: melting point; H_m: melting enthalpy; T_g: glass transition temperature (onset temperature).

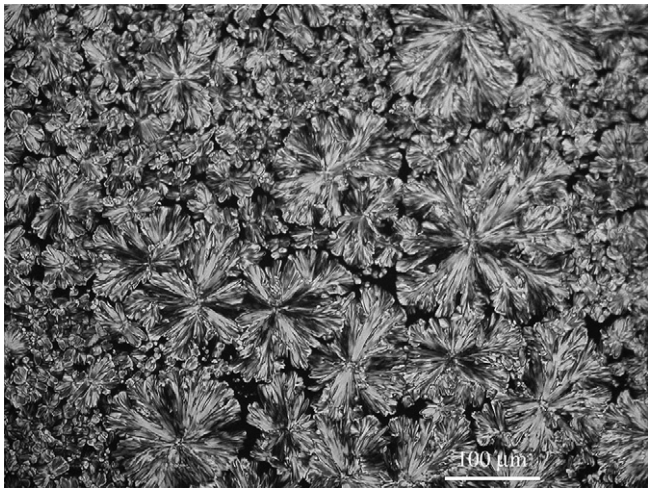

Fig. 5. Polarized optical micrograph of *o*-PETF crystals at a cooling rate of 2 °C/min from equilibrium melting state.

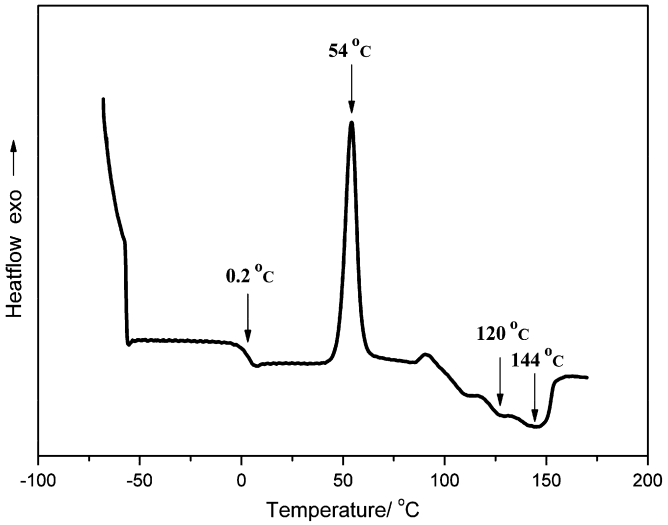

Fig. 7. DSC trace of *o*-PETF quenched at a heating rate of 2 °C/min, N_2.

Comparing the process of cooling from melting state with the quenched from melting state, then heating at a same rate of 2 °C/min (Figs. 3 and 6), three differences were observed between them. First point is the crystallization temperature. In cooling process, the crystallization exothermic peak temperature is 103 °C. However, the cold crystallization temperature is 54 °C (peak value) in quenched then heating process. Experimental results showed that *o*-PETF could grow crystals at 130 °C in melt (Fig. 8 and Table 3). So *o*-PETF had a broad crystallization temperature interval from 54 to 130 °C. Second point is the glass transition behavior. In the cooling process, no glass transition was showed on the DSC curve. When the melt was quenched then heated, a clear glass transition at 0.2 °C (onset temperature) was observed. Because of the high crystallization of *o*-PETF, a great deal of *o*-PETF components formed crystals in the cooling process. The amorphous domains in the system were too small to present a glass transition behavior. But when the sample was quenched from equilibrium melting state, the amorphous state was frozen. So glass transition and crystallization behavior were observed on the DSC curve in the subsequent heating process (Fig. 7). Third point is about the crystalline morphology. Fig. 5 shows that many large dendrites were formed in the cooling process. The crystals formed in quenched then heating process were scrappy and multitudinous (Fig. 6). Because of the large nucleation rate under high super-cooling degree, multitudinous nuclei were formed almost instantly when it entered crystallization temperature interval. Crystalline components grew rapidly on these multitudinous nuclei. The crystals formed were scrappy. In the cooling process with a slowly cooling rate, nucleation rate was small due to the higher nucleation barrier under the lower degree of super-cooling. Only a few nuclei existed in the melt. The crystalline components grew on these nuclei rather than forming nuclei themselves. In that case, large crystals can be formed with comparatively plentiful crystallization time. In other words, we can think about this from the kinetics point of view: in the heating

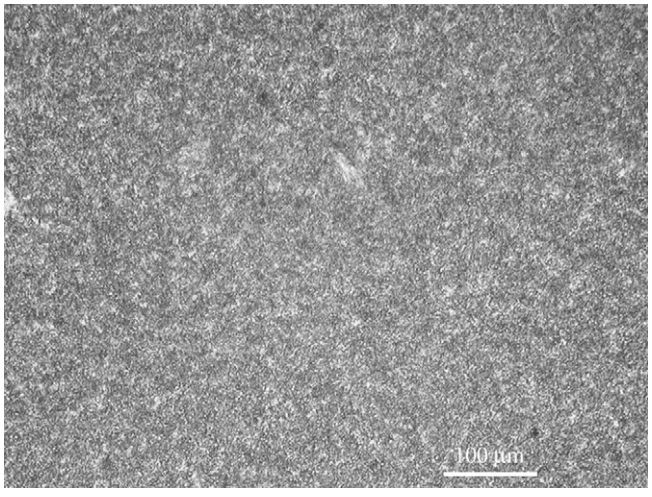

Fig. 6. Polarized optical micrograph of crystals obtained at a heating rate of 2 °C/min with a sample of *o*-PETF quenched.

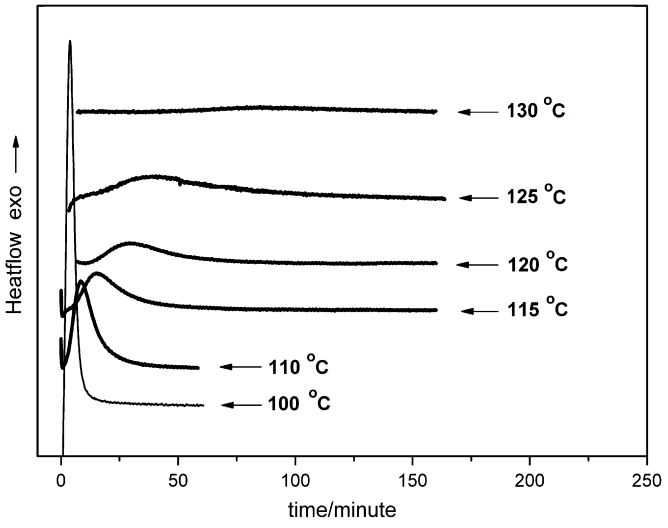

Fig. 8. Isothermal DSC traces of *o*-PETF at different temperatures (100, 110, 115, 120, 125, and 130 °C), N_2.

Table 3
Crystallization enthalpy (H_c) of *o*-PETF in different isothermal crystallization programs

Temperature (°C)	100	110	115	120	125	130
H_c (J/g)	35.4	24.6	16.4	14.6	13.2	8.7

process, many small crystals appeared at early time when sample entered the cold crystallization temperature range of 44–64 °C. When the temperature was subsequently increasing during the heating process, the scrappy crystals formed were going through a re-crystallization phenomenon as observed (Fig. 9).

3.3.2. Crystal reorganization

During the heating of the quenched sample, spherulite growth was observed in the melting process of scrappy crystals with polarized optical microscopy (Fig. 9). In the temperature interval of 120–148 °C, faulty scrappy crystal melting and spherulite growth took place synchronously. This is a crystal reorganization process. Because of the superposition result of exothermic and endothermic behaviors, a shoulder peak was displayed on the DSC curves in the melt transition processes (Fig. 4). These spherulites melted with the increasing temperature. It is the melting of faulty crystals, crystal reorganization (spherulite growth) and melting that make the melt transition broad.

3.3.3. Isothermal crystallization

Isothermal crystallization of *o*-PETF was carried out at different temperatures (Fig. 8). Corresponding crystallization enthalpies are summarized in Table 3. Obviously, crystallization enthalpies decrease with the increase in isothermal temperatures. It indicates that, in the isothermal crystallization processes of *o*-PETF, the higher the temperature, the lower the crystallization enthalpy is. The different crystallization enthalpies at different isothermal temperatures possibly arise from the polydispersity of *o*-PETF. Different length molecular chains may have different crystalline abilities. Some molecular chains or segments cannot pack into crystalline structure at higher temperature. Also it can be understood why there is always amorphous domains in crystalline polymers. In other words, some molecular chains or segments of polymers cannot pack into crystals even at lower temperature. The isothermal crystallization enthalpy at 100 °C is little higher than the crystallization enthalpy obtained in the temperature range of 95–115 °C during the cooling process from the melt at 2 °C/min. The main reason which results in a higher crystallization enthalpy is that it allows the molecules or segments packing into crystalline structure more perfectly at a proper temperature. Fig. 10 shows the dendritic morphology of *o*-PETF grew at 110 °C in melt. In 30 min, the dimensions of crystals formed were about 100–200 μm on the plane direction. The crystallization process was completed in 1 h on the whole. The crystallization degree of *o*-PETF was 74% in 30 min. The average crystalline growth rate at maximum growth direction was about 4.2 μm/min in this period.

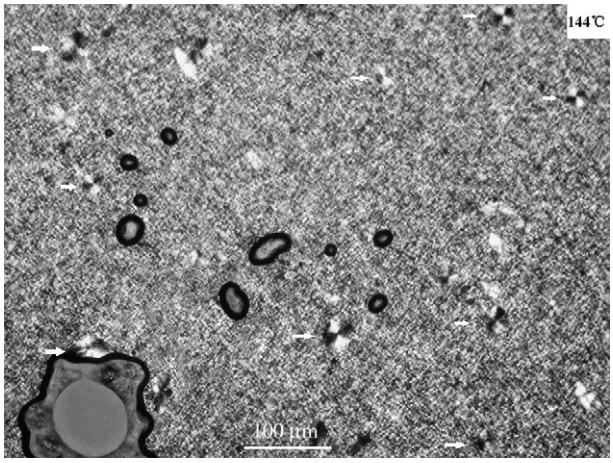

Fig. 9. Polarized optical micrograph of *o*-PETF spherulites indicated with the white arrows.

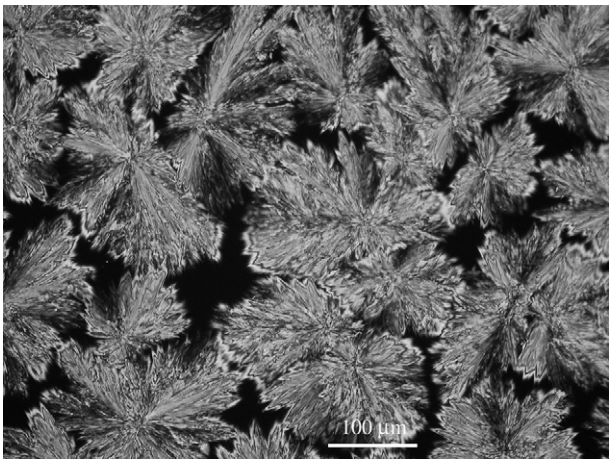

Fig. 10. Polarized optical micrograph of *o*-PETF crystals in an isothermal crystallization process (110 °C).

3.3.4. Effect of fluorine on o-PETF crystallization

o-PET which contains no fluorine, although has a structure similar to *o*-PETF, did not show any crystallization peaks on the DSC curves at different rates (Fig. 11) except glass transition. Also, *o*-PETSF did not show any crystallization behaviors (Fig. 12).

If we only speculate on the unsymmetrical and rigid chemical structure, *o*-PETF should not form crystals easily, just as *o*-PET showed. The high crystallization property of *o*-PETF may be due to the higher mobility of fluorinated polyester chains and dipolar contribution of carbon–fluorine bonds. The fluorinated segments in the polymer backbones reduced intermolecular forces. The correspondingly disengaged chains make themselves easier to pack into the ordered crystalline structure. Dipolar interactions between polymers chains that come from carbon–fluorine bonds may be another crystallization driving force. The fact that higher mobility of fluorinated polyester chains and dipolar interaction between polyester chains coexist in the system seems incompatible. But this is

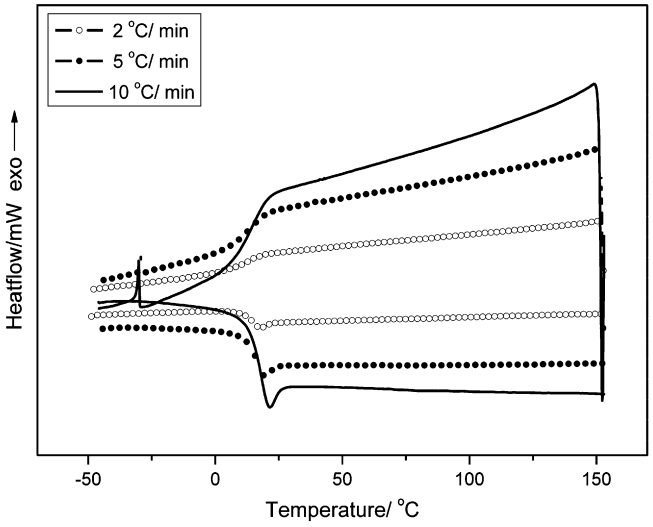

Fig. 11. DSC traces of *o*-PET at cooling/heating rates of 2, 5, and 10 °C/min, N_2.

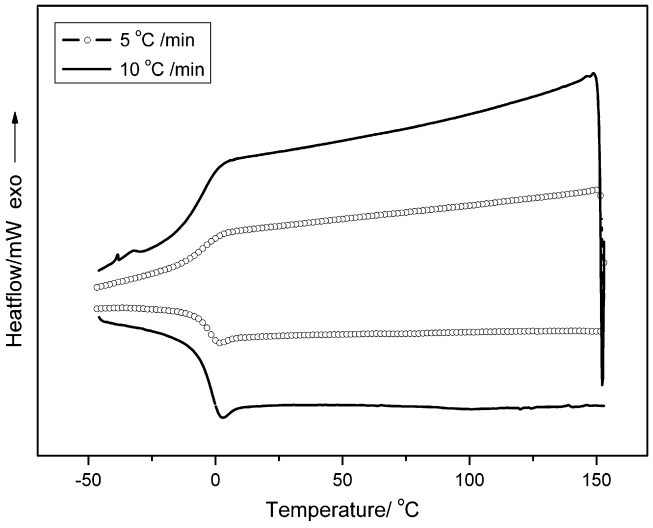

Fig. 12. DSC traces of *o*-PETSF at cooling/heating rates of 5 and 10 °C/min, N_2.

not curious to fluorinated polymers. One example is that the carbon–fluorine bond presents low electronic polarizability and high dipole moment. Another example is that fluorinated materials can possess highly capacitive and even piezoelectric properties. Increasing of rigidity of segmented co-polyester chains with non-fluorinated aromatic segments introduced decrease of the disengaged property of these polymer chains, and therefore crystallization behavior was restrained. Although we cannot eliminate the possibility that the shorter fluorinated sequence length may cause the decrease of crystallization possibility.

4. Conclusions

Highly fluorinated aromatic polyesters were synthesized by a polycondensation reaction of tetrafluorophthalic anhydride with ethylene glycol. The resultant fluorinated polyesters are insoluble in most organic solvents, such as acetone, ethyl acetate, chloroform, THF and trichloromethane. It is soluble in highly polar solvents, such as dimethylsulfoxide, dimethylformamide and dimethylacetamide. *o*-PETF is a highly crystalline polymer with a crystallization enthalpy of 35.2 J/g. It had a broad crystallization temperature interval from 54 to 130 °C. Average crystalline growth rate is 4.2 μm/min at 110 °C in the preliminary 30 min. Spherulite growth was observed in the process of faulty dendrites melt. It represented a crystal reorganization process. Crystalline properties of *o*-PETF can be attributed to the higher mobility of fluorinated polyester chains and dipolar contribution of carbon–fluorine bonds. These make the polymer chains to easily pack into ordered crystalline structures. Increasing of rigidity of segmented co-polyester chains together with the decreasing of the fluorinated sequence length due to the incorporation of the non-fluorinated aromatic segments, have made the polymer chains more difficult to disengage with each other and pack into a crystalline structure, and therefore crystallization behavior was restrained.

Acknowledgments

The authors are grateful for the financial support of research grants 2003CB615600, 20490220, and Natural Science Foundation of China (20404006), excellent young scientist awarded fund of Shandong province (2004BS04018).

References

[1] (a) Wilson LM, Griffin AC. Macromolecules 1994;27:1928;
(b) Wilson LM, Griffin AC. Macromolecules 1994;27:4611.
[2] (a) Powell KT, Cheng C, Wooley KL, Singh A, Urban MW. J Polym Sci Part A Polym Chem 2006;44(16):4782;
(b) Powell KT, Cheng C, Gudipati CS, Wooley KL. J Mater Chem 2005; 15(48):5128;
(c) Cheng C, Wooley KL, Khoshdel E. J Polym Sci Part A Polym Chem 2005;43(20):4754;
(d) Gudipati CS, Finlay JA, Callow JA, Callow ME, Wooley KL. Langmuir 2005;21(7):3044;
(e) Gudipati CS, Greenlief CM, Johnson JA, Prayongpan P, Wooley KL. J Polym Sci Part A Polym Chem 2004;42(24):6193;
(f) Gan DJ, Mueller A, Wooley KL. J Polym Sci Part A Polym Chem 2003;41(22):3531;
(g) Mueller A, Kowalewski T, Wooley KL. Macromolecules 1998;31(3): 776.
[3] Gouinlock Jr EV, Verbanic CJ, Schweiker GC. J Appl Polym Sci 1959;1: 361.
[4] Schweiker GC, Robitschek P. J Polym Sci 1957;XXIV:33.
[5] Pilati F, Manaresi P, Toselli M. J Polym Sci Part A Polym Chem 1990;28: 3047.
[6] Pilati F, Bonora V, Manaresi P, Munari A, Toselli M. J Polym Sci Part A Polym Chem 1989;27:951.
[7] Pilati F, Toselli M, Vallieri A, Tonelli C. Polym Bull 1992;28:151.
[8] Toselli M, Pilati F, Fusari M, Tonelli C, Castiglioni C. J Appl Polym Sci 1994;54:2101.
[9] Alexaner YB, Olga SS, Anatoly JG. Macromol Chem Phys 1996;197: 1021.
[10] Levi M, Turri S. J Polym Sci Part A Polym Chem 1998;36:939.
[11] Gitina RM, Zaitseva EL, Yakubovich AY. Russ Chem Rev (Engl Transl) 1971;40(8):679.

[12] Keller TM. J Polym Sci Part A Polym Chem 1984;22:2719.
[13] Maruyama Y, Kakimoto MA, Imai Y. J Polym Sci Part A Polym Chem 1986;24:3555.
[14] Zhang L, Huang WY. J Fluorine Chem 2000;1–2:55.
[15] Kang SH, Luo JD, Ma H, Barto RR, Frank CW, Dalton LR, et al. Macromolecules 2003;36(12):4355.
[16] Mera AE, Griffith JR, Armistead JP. Polym Prepr (Am Chem Soc Div Polym Chem) 1990;31(1):318.
[17] Choi EJ, Hill DJT, Kim KY, ODonnell JH, Pomery PJ. Polymer 1997; 38(14):3669.
[18] Hauptschein M, O'Brien JF, Stokes CS, Filler R. J Am Chem Soc 1953; 75:87.